PAPER

Development of a sensor device with polymer-coated piezoelectric micro-cantilevers for detection of volatile organic compounds

Development of a sensor device with polymer-coated piezoelectric micro-cantilevers for detection of volatile organic compounds

Waqar M Ahmed[1] , **Ruud J A Steenwelle**[2], **Hugo H Knobel**[3],
Alan Davie[4], **Ron Steijvers**[4], **Fred Verhoeckx**[4], **Royston Goodacre**[5] ,
Stephen J Fowler[1,6] , **A J H M Rijnders**[2], **Tamara M Nijsen**[4] **and on behalf of the BreathDx consortium**

[1] School of Biological Sciences, Faculty of Biology, Medicine and Health, University of Manchester, Manchester, United Kingdom
[2] Faculty of Science and Technology, University of Twente, Enschede, The Netherlands
[3] Eurofins Materials Science Netherlands BV, Eindhoven, The Netherlands
[4] Philips Research, Royal Philips B.V., Eindhoven, The Netherlands
[5] Institute of Integrative Biology, Department of Biochemistry, University of Liverpool, Liverpool, United Kingdom
[6] Manchester Academic Health Science Centre, Manchester University Hospitals NHS Foundation Trust, Wythenshawe, United Kingdom

E-mail: tamara.nijsen@philips.com

CrossMark

Abstract

Exhaled breath contains thousands of volatile organic compounds (VOCs), some of which have been associated with respiratory disease. We describe a sensor device with an array of eight polymer-coated piezoelectric micro-cantilevers (two of each polyacrylic acid, polyethylenimine and polyethylene glycol and two uncoated cantilevers) and an electronic resonant frequency readout, designed for analysis of VOCs. We have measured the system's response to temperature (24 °C to 40 °C), pressure (200 mmHg to 760 mmHg), and humidity (10% to 50% RH), evaluated the reproducibility of measurements between micro-cantilevers ($n = 3$), and tested the stability of the system over six months. By measuring the frequency shift of the resonating micro-cantilevers, and using the inflection point of a fitted sigmoid model, we show that acetone, ethanol, octane are distinguishable from one another, with a measurement limited of detection of 1568, 383, and 87 ppmv, respectively. From interpolation of the electronic readout, we found the lowest estimated measurement to be 5 ppmv (acetone on polyacrylic acid). We have also shown that polar mixture (acetone, ethanol, and water) and non-polar mixture (increasing octane concentration and decreasing polar mixture constituents) can be differentiated.

Keywords: volatile organic compounds, sensor, cantilever, breathdx

S Supplementary material for this article is available online

(Some figures may appear in colour only in the online journal)

Introduction

Thousands of volatile organic compounds (VOCs) have been identified in human samples and from both exogenous and endogenous origins, and many methods have been developed to utilize VOCs for disease diagnosis (Pleil *et al* 2013, de Lacy Costello *et al* 2014, Amann *et al* 2014). Sampling VOCs is non-intrusive, and like saliva and urine sampling, can be collected with relative ease, compared to invasive methods such as blood or sputum collection (Navazesh *et al* 1993, Beauchamp and Pleil 2013). Some VOCs have been associated with lung disease and investigated as diagnostic markers (Miekisch *et al* 2004, Haick and Cohen-kaminsky 2015, Bos *et al* 2016, Ahmed *et al* 2017). The presence of saturated and unsaturated hydrocarbons (i.e. increased non-polar compounds) are often reported in relation to lung inflammation and infection (Ibrahim *et al* 2011, Bos *et al* 2014). The hospital environment also contains VOCs from decontamination products and volatile inhalational anaesthetics (Bessonneau *et al.* 2013).

A diverse array of instruments for analysing breath VOCs are available and provide highly sensitive and accurate identification (Lourenço and Turner 2014, Beale *et al* 2016). Hyphenated mass spectrometry (-MS) methods, where chemical compounds are subjected to electron or chemical ionization, are commonly used in breath research, typically paired with sample separation methods such as gas chromatography (GC) (Basanta *et al* 2012b), proton transfer reaction (PTR) (White *et al* 2013), and selected ion flow tube (SIFT) (Smith and Španel 2005). Analyte separation is not carried out in SIFT-MS and PTR-MS, and can therefore be used for real-time analysis. GC-MS is usually coupled with a pre-concentration technique such as solid phase micro-extraction (SPME).These such instruments are generally expensive, bulky and heavy, and require a high-level maintenance and specialist operation. The size and cost can be reduced by using novel ion mobility spectrometry (IMS) devices adapted for clinical breath analysis (Basanta *et al* 2010, Rabis *et al* 2011), though instruments have complicated installation and require periodic maintenance by specialists.

Electronic nose (eNose) gas sensors are low cost, and easy to use, when compared to other methods. The wide range of eNose sensors and their applications have been reviewed before (Konvalina and Haick 2014, Wilson 2015). Recent developments in on-line VOC sensors support their future potential use in the clinic, such as disposable tubes with integrated sensors (Wu *et al* 2016), and integration of eNose sensors with spirometry (de Vries *et al* 2015). The clinical feasibility of such devices are yet to be determined.

Depending on the sensor's mechanism of action, eNoses are designed to be either chemically selective for a specific VOC (lock and key) or chemical group, or can differentiate between chemical patterns. Signal processing algorithms can be performed during (on-line analysis) or immediately after sampling VOCs (off-line) for clinical interpretation (Gromski *et al* 2014), where on-line analysis is usually preferred for fast and efficient analysis in a clinical setting. Micro-electro-mechanical-system (MEMS) sensors have shown potential

for VOC detection and classification of chemical groups (Yoshikawa *et al* 2009). Sensor chips can be mass produced at low cost and can be interchangeable with other chips for single use or for a different panel of sensors. One group of MEMS type sensors called acoustic wave detectors have shown potential in breath VOC analysis. A study by Phillips *et al* used a GC-SAW device to profile patients with pulmonary tuberculosis (Phillips *et al* 2012).

Micro-cantilever-based sensors are common and have been developed for VOC analysis, where studies have shown their good sensitivity and specificity towards VOC samples (Maute *et al* 1999, Lange *et al* 2002, Xu *et al* 2010, Pettine *et al* 2012, 2013). Gerber *et al* have shown separation between alkanes by carbon number using principal component analysis (Yoshikawa *et al* 2009). However, a purpose-built integrated MEMS device for breath analysis in large scale clinical trials is required and to our knowledge, no such micro-cantilever-based sensor device is available for clinical use. Such a system should be stable between multiple measurements and show chemical specificity with high sensitivity, typically down to ppmv-ppbv concentrations as breath contains VOCs within this concentration and it is therefore essential to achieve this detection range with eNose devices (Rattray *et al* 2014).

Here, we describe the development of a stand-alone integrated MEMS device for VOC profiling with an electronic resonant frequency output that measures several resonating micro-cantilevers simultaneously. We describe how this test setup responds to changes in the environment; e.g. temperature, relative humidity and atmospheric pressure. VOC concentrations were then measured with the sensor to assess chemical differentiation, detection sensitivity, and short-term and long-term measurement reproducibility of micro-cantilevers. We chose to test acetone as it is a common breath constituent; ethanol as it is used in hospital decontamination products, and octane as this was identified as a potential marker for acute respiratory distress syndrome (de Lacy Bessonneau *et al* 2013, Bos *et al* 2014, de Lacy Costello *et al* 2014).It is important to note that these compounds are non-specific and have been identified from various sources. For example, acetone levels are increased in diabetics and decreased in heart failure patients (Ghimenti *et al* 2013, Biagini *et al* 2017).

Materials and methods

Sensor micro-fabrication and resonant frequency output

In this application we employ a single micro-cantilever beam arrangement (length 200 μm × width 100 μm, thickness 2 μm), with one end glue-bonded onto the electrode. Micro-cantilevers were fabricated and assembled on a silicon-on-insulator wafer, starting with thermal oxidation and deposition and patterning of the bottom electrode, followed by pulsed laser desorption of the PZT layer and deposition and patterning of the top electrode and gold patch, patterning of the PZT layer, and finally patterning and release of the micro-cantilever. Further information about the micro-cantilever fabrication and stability can be found in our previous work (Dekkers *et al* 2009). Figure 1 shows the layers as described
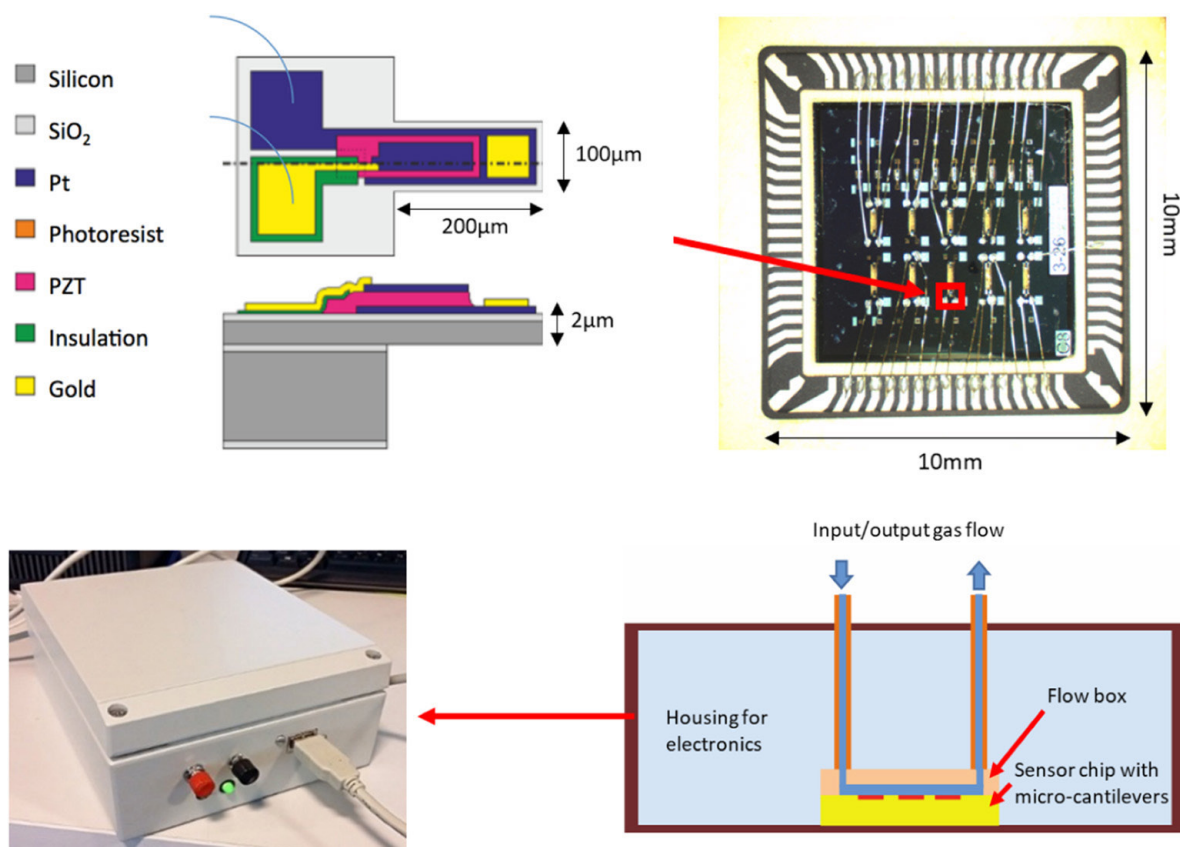
Figure 1. Sensor mechanism layout and sensor housing images. Top left: 2D illustration showing the top and side view plan of a single micro-cantilever with colours highlighting various fabricated layers for a non-coated micro-cantilever (where SiO_2 is silicon dioxide, Pt is platinum, and PZT is lead zirconate titanate). Top right: an image ($\times 10$ magnification) of the sensor chip (10×10 mm) with multiple cantilevers with a single micro-cantilever highlighted in red. Bottom right: A schematic of the flow box (internal volume 300 µl) where gas is directed above the sensor chip. Bottom left: the housing for the electronics suitable for portable on-site analysis (148×210 mm).

above, and the microscope image of the chip carrier forming the micro-cantilever sensor array (1 mm × 1 mm).

The electronic connection between the micro-cantilever and chip carrier were made by wire bonding. To give the sensor the ability to chemically interact with VOCs (as well as changes in mass and stiffness), functionalized polymer layers were spotted (density 1 g cm^{-3}, thickness 50 nm) onto the tip of each cantilever using the FEMTO (Fluidics Enhanced Molecular Transfer Operation) process with a Nano eNabler molecular printing system (BioForce Nanosciences, USA) (Alvarez and Lechuga 2010, Fu and Ayazi 2010).

Selected polymer coatings included polyacrylic acid (PAA), polyethylene glycol (PEG), and polyethylenimine (PEI). Cantilevers with no polymer coating were included for reference measurements (control). Two micro-cantilevers with the same coating were included on the sensor chip ($n = 8$). Polymers coated onto micro-cantilevers were chosen based on their interaction with a range of VOCs with varying chemical properties (including polarity and electrostatic interactions).

The resonant frequency is dependent on the mass applied to a micro-cantilever. Our system measures the baseline resonant frequency (f) and tracks changes in resonance (under microprocessor control) by continuously monitoring the phase shift in signals applied to the micro-cantilever. This allows for

tracking of the frequency shift for each cantilever (Δf) sequentially, and in real-time (within milliseconds per step response).

In theory, when the micro-cantilevers are exposed to a gas containing VOCs, molecules bind to the surface of the cantilever, or absorb into the polymer coating, thereby causing a measurable increase in mass, causing a decrease in f. Additionally, as with all resonance-based devices, changes in micro-cantilever stiffness caused by surface stresses change the spring constant and therefore also impact Δf (Waggoner and Craighead 2007). Absorption of VOCs into polymer receptor layers generally decreases the stiffness and therefore lowers the frequency. In this way, the stiffness effect amplifies the mass generated resonance frequency shift.

Measurements of environmental changes

Variations in ambient pressure, humidity, and temperature were measured. Controlled and ambient measurements were performed. Controlled measurements included a temperature range from 24 °C to 40 °C (as the temperature of breath is within this range), pressure range from 760 mmHg down to 200 mmHg (to mimic atmospheric pressure fluctuations), and relative humidity from 10% to 50% (to reflect low humidity in a clinical environment). Sample humidification
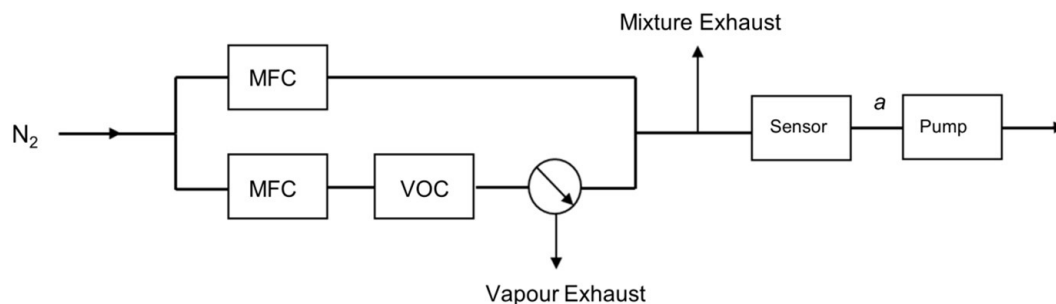
Figure 2. Gas delivery system used to flow a concentration of a VOC in dry N_2 through the sensor. In summary, N_2 gas is first split between two programmable mass flow controllers (MFC). One stream is carried towards a stainless-steel canister, containing a chemical liquid standard (VOC), to achieve a saturated gas vapour mixture of the selected VOC in N_2. A toggle valve at this point allows the vapour generated to be redirected to an exhaust. The vapour mixture is then further diluted into the second stream of carrier N_2 gas to create a concentration ratio mixture. The diluted stream is then pumped through the device flowbox (housing the sensor chip) at a flow rate of 20 ml min^{-1}. Surplus vapour is expelled through an exhaust. A conditioned thermal desorption tube was added between the sensor and pump (location marked 'a') when required.

involved increasing the gas mixing ratio of water in dry N_2. Measurements of ambient environmental changes were performed over eight hours, and simultaneously monitored using a calibrated barometric datalogger (Extech SD700, FLIR Systems, USA) to compare sensor response with the surrounding environment. The datalogger was set to acquire data every 5 s.

VOC measurements

Laboratory standard chemicals (Sigma Aldrich, UK) of octane, acetone, and ethanol (>95% purity) were used for analysis. Acetone is ubiquitous in breath. Ethanol and octane are of interest as high concentrations may originate from microbial metabolism and lipid peroxidation, respectively (Bos *et al* 2014; Bos *et al* 2013). A controlled mixture of VOC vapour in dry N_2 at a constant flow (20 ml min^{-1}) was purged onto the micro-cantilever array using the system illustrated in figure 2. This flow remained constant throughout all runs. Ratios of 0.66%, 1%, 2%, 3%, 4%, 5%, and 10% of saturated VOC vapour to N2 were measured. VOC concentrations in ppmv were calculated using this ratio and Antoine equation and constants specific to each VOC (NIST Standard Reference Database No. 69).

Thermal desorption-gas chromatography-mass spectrometry (TD-GC-MS) was carried out as part of the quality assessment of the air surrounding the system, and identification of compounds running through the sensor flowbox. Here, thermal desorption tubes were used which were packed with Tenax TA and Carbograph 5TD, and GC-*tof*-MS chromatographic and MS acquisition parameters were set as described elsewhere (van Oort *et al* 2017). The tube was placed in-line between the sensor exhaust and the pump. A total volume of 20 ml of the gas mixture from the sensor was drawn onto the tube (20 ml min^{-1}).

Signal post-processing

Resonant frequency data acquired during on-line measurement were evaluated off-line to develop suitable post-processing methods. All post-processing and data analysis were

carried out in Matlab (Mathworks Inc., USA, version R2015b). Each Δf observation was centred by the initial frequency $f0$ ($\Delta f/f0$). The $\Delta f/f0$ vector was then corrected to remove systematic drift by subtracting a fitted polynomial curve across all baseline measurements for each experimental run.

To plot concentration curves, a $\Delta f/f0$ response vector was extracted for each concentration and polymer coating combination. The magnitude of the response curve was then calculated and used for plotting concentration curves using the following equation:

$$Z = \sqrt{\sum_{i=1}^{N} \Delta f_i^2} \qquad (1)$$

where the magnitude (Z) of the response vector is the square root of the sum of $\Delta f/f0$ values (denoted in equations (1) and (2) as Δf). For easy integration into on-line data processing, a time-independent value extracted from a suitable model was required. A reverse sigmoid model was applied to the $\Delta f/f0$ vector:

$$S(\Delta f) = c + \frac{a}{1 + e^{(\Delta f - b)}} \qquad (2)$$

where a, b, and c are the curve fitting coefficients and S is the fitted sigmoid curve. The final value was extracted from the point at which the $\Delta f/f0$ vector intersected the inflection point (*IP*) of the sigmoid curve (where $f'' = 0$). Two additional features (adapted from the linear extrapolation method) described previously (Chen and Chang 1991, McDowall and Dampney 2006) were extracted from the curve—the 'adsorption' point (*AP*) and the 'saturation' (*SP*) point, where *AP* is defined as the point from which $\Delta f/f0$ decreases below the upper horizontal asymptote, and *SP* as the point from which $\Delta f/f0$ no longer decreases (i.e. the sensor coating is saturated).

The time taken to reach *SP* from *AP* (t^S) was used in fingerprinting analysis. To assess how well the sigmoid models original data, the area under the curve (AUC) for each vector and root mean squared error (RMSE) were calculated. Arbitrary thresholds were set to accept or reject resulting data where the model was used. A good match was indicated by an AUC > 80%, and no RMSE outliers.

The mean *IP* and mean t^S of three replicates were used to develop heat maps to compare micro-cantilever 'fingerprints' visually for each VOC. The input values for the heat maps were normalised by sum and feature-scaled across polymer observations to generate a value between 0 and 1, where 1 showed the maximum intensity observed for a VOC. To exclude the dominant effect of concentration for VOCs with high vapour pressure, data with similar VOC concentrations (acetone at 1568 ppmv; ethanol 1158 ppmv; water 1303 ppmv and octane 1316 ppmv) were used to generate heat maps and assess reproducibility. Additionally, principal component analysis (PCA) was carried out where samples were represented as individual VOCs or VOC mixtures, and micro-cantilevers represented the features. Data were mean centred prior to PCA. All the data were then represented across 2 principal components (PCs). For comparing between mixtures, polar and non-polar mixtures were made. The polar mixture included acetone, ethanol, and water, whereas the non-polar mixture contained octane. The ratio of each mixture was changed (20%, 30%, and 40% in N_2 for each mixture) and evaluated by PCA.

Intra-run repeatability (octane only) and inter-run reproducibility were assessed for each polymer by calculating the relative standard deviation (% RSD) across three replicates runs. To assess the effect of long-term use of the same chip (0 and 180 d) and differences between duplicate cantilevers with the same coating, the *IP* median and interquartile range (IQR) were compared between each sensor group, with *t*-tests performed to test significance ($\alpha = 0.05$).

Results

Response to environmental changes

Measurements of temperature, humidity and pressure were performed in a pressure-controlled oven. The change in frequency ($\Delta f/f0$) of a control micro-cantilever in response to environmental changes correlated with that of a coated micro-cantilever, as shown in figure 3. The response for both control and coated micro-cantilevers also correlated with the stepwise change in environmental stimuli i.e. decreasing temperature (sensitivity of 0.05 Hz °C^{-1}), increased pressure (−ve), and increased relative humidity (sensitivity of 0.1 Hz/%RH).

Measurements of ambient room temperature, humidity, and pressure were also carried out. Temperature changes showed an inverse relationship with $\Delta f/f0$ signal over a period of approximately 8 h (figure 4). As this included uncontrolled environmental changes, the acquired signal will be influenced by ambient humidity and pressure. However, in our case, no discernible relationship was shown with humidity or pressure after measurement, most likely due to the low ambient fluctuations.

Detection of VOCs

Vapour mixtures of acetone, ethanol, and octane chemical standards in dry N_2 were purged onto the micro-cantilever array with
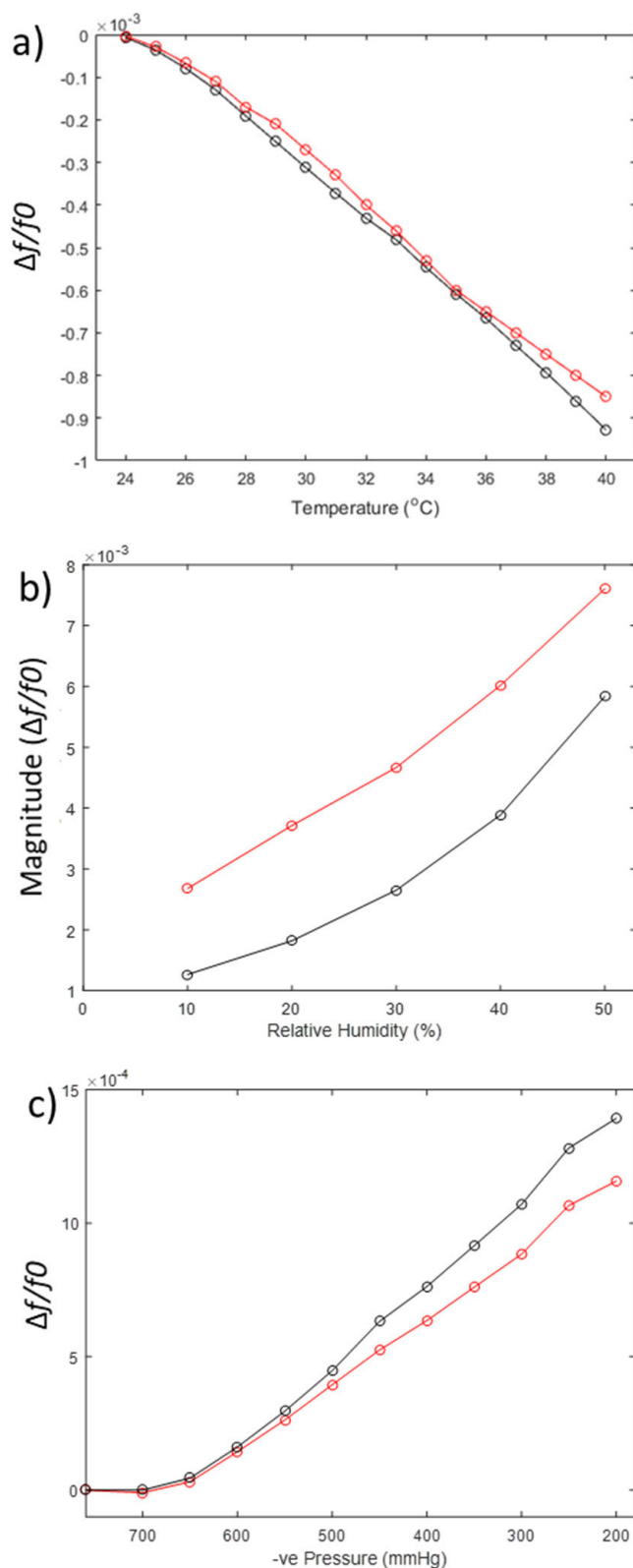

Figure 3. Single measurements showing a $\Delta f/f0$ response to environmental conditions: (a) increasing oven temperature from 24 °C to 40 °C (1 °C intervals); (b) increasing relative humidity from 10% to 50% (10% intervals); (c) pressure range from 760 to 200 mmHg (50 mmHg intervals). All charts show a control (black) and coated (red, PEG) micro-cantilever response as examples.
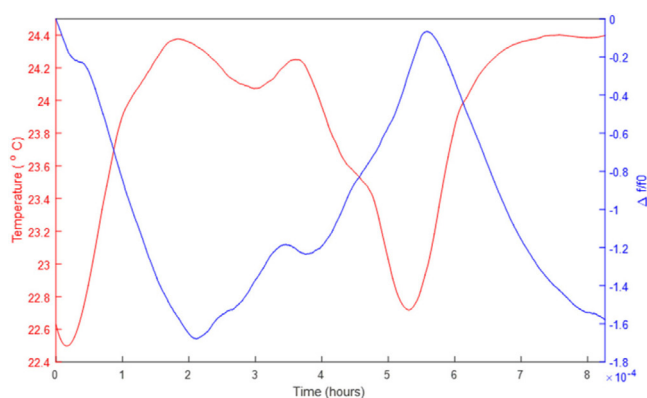
Figure 4. Ambient room temperature readings (red line, *y* axis on the left) and $\Delta f/f0$ measurement of a control micro-cantilever (blue line, *y* axis on the right) aligned by time over a period of approximately 8 h.

data acquired in real-time. Dry N_2 was used to assess the sensors response to single chemical vapours without introducing moisture. Coated micro-cantilevers showed a greater $\Delta f/f0$ response to VOCs when compared to control micro-cantilevers. Analysis by TD-GC-MS confirmed the presence of ethanol, acetone, and octane, and revealed no artefact VOCs from the gas delivery system or the surrounding air. However, we found a 5 to 10 min dry N_2 purge was not sufficient to clear the system *between* gas samples, which may be attributed to the high vapour concentration. Compound peaks from the mixture gas are shown in the chromatogram (S1) (stacks.iop.org/MST/31/035103/mmedia). The minimum measured concentration detected from our current gas delivery system was for octane at 87 ppmv. The estimated measurement detection limit by linearly interpolating the synthesiser step size signal-to-noise ratio (SNR) using a $\Delta f/f0$ vector (acetone on PAA) was estimated at approximately 5 ppmv. These lower limits are high when compared to other studies which have LODs in the ppb range.

An increase in $\Delta f/f0$ in response to all VOCs is shown by all polymer-coated micro-cantilevers, where PAA has the weakest response, and PEG the strongest response, with the exception of octane where PEI shows the strongest response above 263 ppmv. The uncoated control micro-cantilever interacts with acetone above 4737 ppmv, whereas for ethanol, the control remains unresponsive throughout all concentrations (measured up to 5789 ppmv). Similarly, an increase for the control micro-cantilever is also shown for octane above 396 ppmv. Real-time micro-cantilever response curves and concentration curves ($n = 3$) for each VOC are shown in figure 5.

VOC fingerprinting

2D heat maps were generated for each VOC and polymer coating pair for visual representation of fingerprints, using the mean *IP* and t^S data. Heat maps are shown in figure 6.

According to the heat maps, all control micro-cantilevers had the lowest concentration in response to VOCs when compared to all polymer-coated micro-cantilevers (PAA, PEI, and PEG). As a consequence of the response being minimal the sigmoid model failed to fit to the data (as they were outside

the RMSE and AUC threshold criteria), and therefore their *IP* was set to zero. This was also the case for the PAA polymer response to water. It is important to note that we also observed high concentrations of water invoke a response on PAA (data not shown), which may be attributed to increased mass on the cantilever.

With regard to the heat map showing t^S fingerprints (figure 6(b)), darker colours indicate an increased length of time to reach *SP*. According to the heat map, the fastest t^S was shown by octane (4.63 min), with the fastest reading on PEI (4.57 min), in comparison to other VOCs (acetone 9.04, ethanol 6.82, and water 6.94 min). It is therefore evident that octane has a better affinity for PEI compared to other polymers, most likely due to its low polarity and larger surface area. On average, PEG was slowest to respond from the three coated micro-cantilevers (PEG 7.97, PEI 7.26, and PAA 7.12 min).

PCA was carried out and the scores plot (figure 7) showed separation between individual VOCs in N_2 where water separated across the first PC (figure 7(a)), with octane and ethanol samples being separated in the second PC. Mixture samples were also analysed with PCA with both PC1 and PC2 showing variation due to sample concentration. A corresponding PCA loadings biplot is provided in S2 and shows the importance of polymers responsible for separating VOCs.

Measurement reproducibility

Relative standard deviations (RSDs) for repeatability measurements (within run) and reproducibility measurements (between runs) are summarised in table 1. Inter-run reproducibility results showed measurements with PAA were the most reproducible in comparison to other coatings (mean RSD of 13.5%), and acetone compared to other VOCs (mean RSD of 9.2%).

Three replicates were used to calculate the RSD for each pair (VOC and polymer-coated microcantilever), and only octane was used to assess intra-run repeatability. Water vapour did not react with PAA at this concentration therefore no signal was extracted.

No clear difference was found between baseline ($n = 9$, median -5.80×10^{-6}, IQR 1.93×10^{-6}) and measurement after 180 d ($n = 9$, median -7.00×10^{-6}, IQR 3.28×10^{-6}, paired t-test $p = 0.553$ for difference). Comparisons of $\Delta f/f0$ readings between two micro-cantilevers with the same coating were also made. In this case, All VOCs were included, and groups consisted of sensor one and sensor two (paired within measurement) for micro-cantilevers coated with PEI and PAA. Between PEI sensor one ($n = 12$, median -4.44×10^{-6}, IQR 2.70×10^{-6}) and sensor two ($n = 12$, median -1.46×10^{-6}, IQR 2.54×10^{-6}) a difference 2.98×10^{-6} *Hz* was found where sensor two had a low $\Delta f/f0$ in comparison (paired t-test $p \leqslant 0.001$). Similarly, between PAA sensor one ($n = 8$, median -3.13×10^{-6}, IQR 1. 80×10^{-6}) and sensor two ($n = 8$, median -1.62×10^{-6}, IQR 2.00×10^{-6}) the results indicated a difference of 1.51×10^{-6} *Hz* ($p = 0.0039$). A summary table of the above reproducibility analysis is shown in the supplementary information (S4).
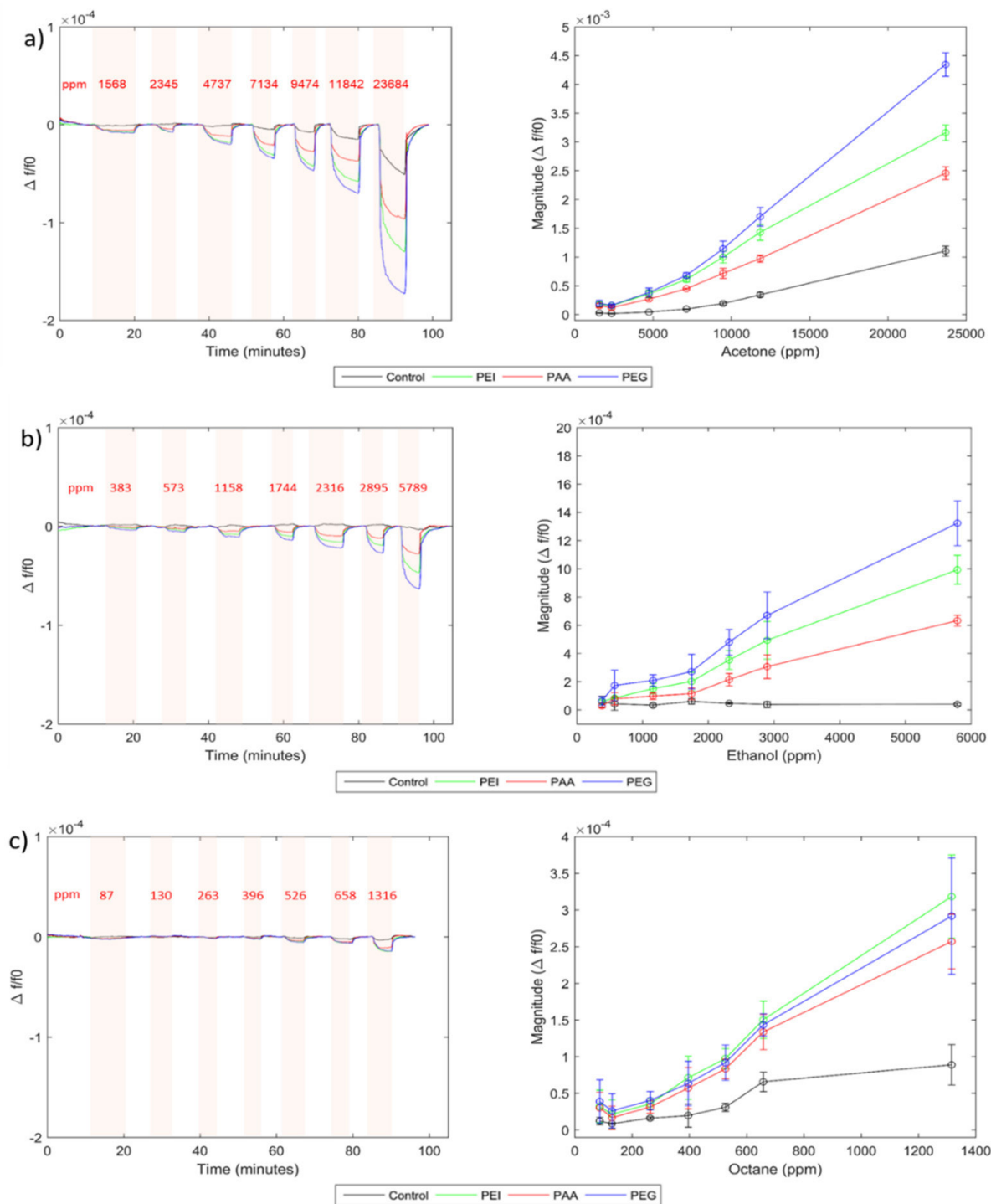
Figure 5. Time series (left) and concentration curve (right) plots of acetone (top), ethanol (middle), and octane (bottom). All graphs show four cantilever $\Delta f/f0$ responses (coloured). Time series plots were corrected for sensor response drift and the magnitude for each $\Delta f/f0$ response curve calculated to form concentration curves from three sequential runs (where a circle is the mean response, and positive/ negative error bars show standard deviations).

Discussion

We have developed an integrated sensor device with a simultaneous readout of eight piezoelectric micro-cantilevers coated with three different polymers coatings, tailored towards breath VOC analysis. We achieved this by measuring VOCs commonly found in exhaled breath gas. In addition, we evaluated the system's performance by assessing reproducibility of measurements.

After continuous 8 h run without flow, we found the $\Delta f/f0$ signal matched that of temperature fluctuations. This suggests that temperature has a direct effect on systematic drift during measurement and is also consistent with controlled measurements taken from 24 °C to 40 °C. This result shows
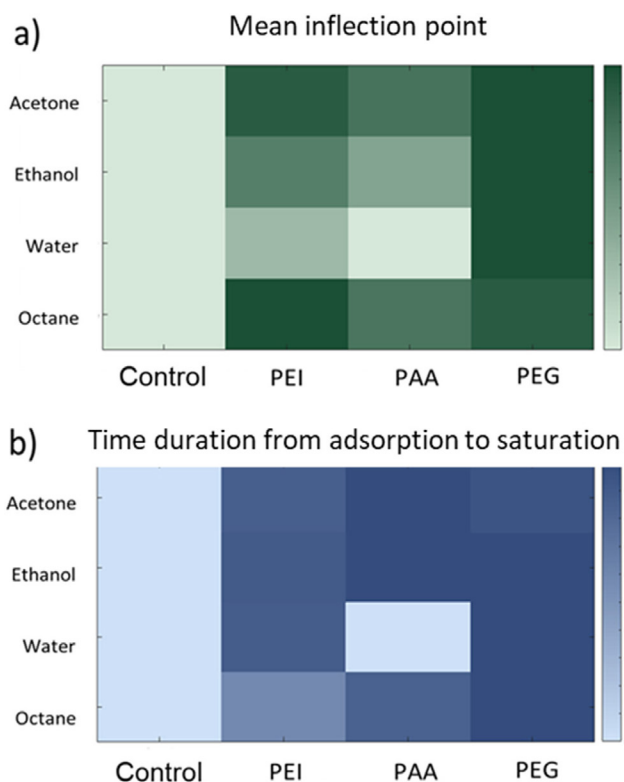
Figure 6. Heat maps with each rectangle showing the intensity of (a) the mean inflection point, and (b) or time taken to reach the saturation point from the adsorption, of each VOC (at a specific concentration) to illustrate the fingerprinting potential of the selected cantilevers.

temperature must be monitored and data used to correct for fluctuations in signal drift, especially as temperature of breath gas and the surrounding clinical environment around the sensor will not be constant.

As expected, the control micro-cantilevers exhibited a low $\Delta f/f0$ shift in comparison to coated micro-cantilevers. Regarding acetone a notable increase in $\Delta f/f0$ is observed for control micro-cantilevers, which may be attributed to increased mass on the micro-cantilevers from vapour mixtures with high ppmv concentration, explained by increased electrostatic interaction between acetone molecules on the silicon dioxide layer of the micro-cantilever.

In combination, all polymer coated cantilevers were able to differentiate VOCs. According to intensity patterns on the IP heat map, octane and acetone were not visually different by PEI or PAA, and required PEG to differentiate the two VOCs, whereas ethanol and water could be differentiated by PEI and PAA coated micro-cantilevers. The overall high intensity of PEG (compared to PAA and PEI) for polar VOCs may be due to hydrogen bonding on the O–H termini of the PEG polymer surface, whereas the comparatively lower intensity for octane due to its low polarity and therefore low chemical affinity, may only exhibit weak Van der Waals forces due to its low chemical affinity for the PEG surface. Chemical interactions, which are based on solubility properties of the polymer coating, cause swelling and deswelling and therefore changes in resonance. As it was possible to extract additional features, the time taken for VOC $\Delta f/f0$ signals to reach 'saturation'
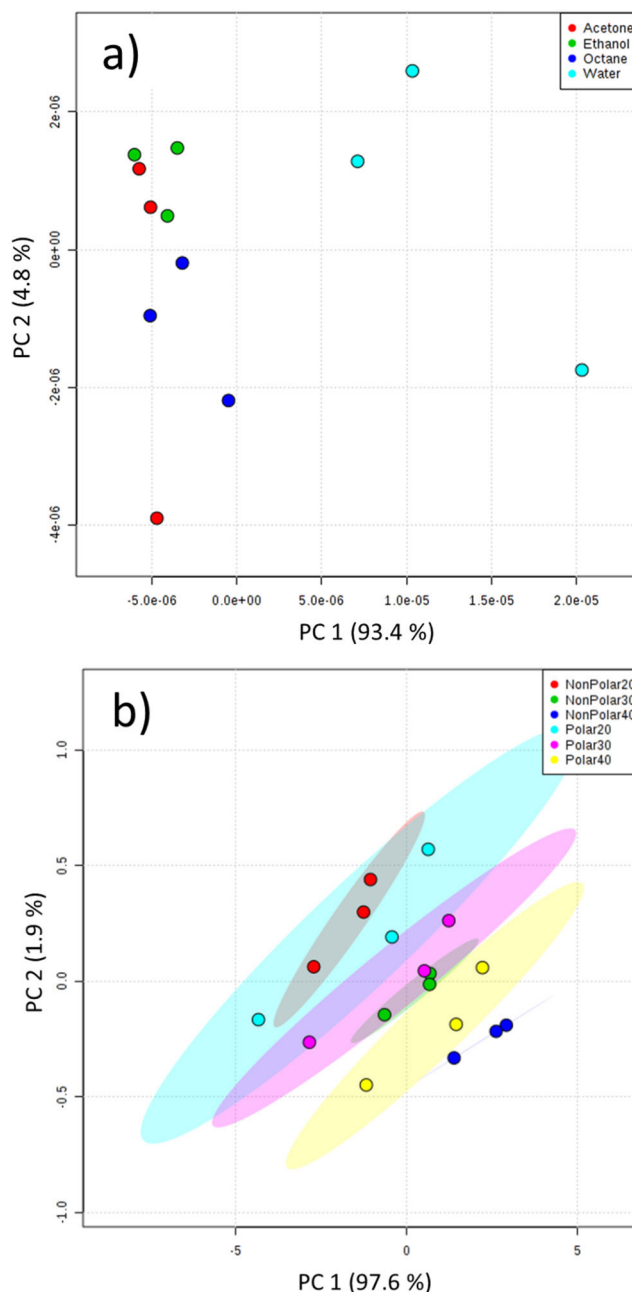

Figure 7. PCA score plots of sensor response to vapour of (a) individual VOC gas samples at similar concentrations where colours indicate different VOCs (the explained variance for each PC is provided in the plots in parentheses and the total (TEV) = 98.2%), and (b) polar and non-polar gas mixture samples where colours indicate are different relative concentrations (20%, 30%, or 40%) of either polar or non-polar mixtures (TEV 99.5%).

were measured with a maximum time of 10 min. Improved response times may be achieved by increasing the electronic gain setting.

With regard to PCA results, data separation of water samples were due to the PAA coated micro-cantilever and comparably increased $\Delta f/f0$ of PEG and PEI for other VOCs, as also shown by the heat maps. PCA of VOC mixtures revealed separation between polar and non-polar mixtures. It is interesting to note that this observation is more apparent at larger

Table 1. Mean Δf ($\pm$SD) and relative standard deviation (% RSD) for each polymer coated microcantilever.

		PEI	PAA	PEG
	VOC (ppmv)	Mean ($\pm$SD) %RSD	Mean ($\pm$SD) %RSD	Mean ($\pm$SD) %RSD
Intra-run repeatability ($\times$10)	Octane (1316)	-2.7×10^{-6} ($\pm 8.6 \times 10^{-7}$) **31.9**	-2.0×10^{-6} ($\pm 8.4 \times 10^{-7}$) **41.8**	-2.4×10^{-5} ($\pm 4.6 \times 10^{-6}$) **19.0**
Inter-run reproducibility ($\times$3)	Water (1303)	-6.6×10^{-6} ($\pm 1.4 \times 10^{-6}$) **21.1**	—	-2.1×10^{-6} ($\pm 6.3 \times 10^{-6}$) **29.3**
	Acetone (1568)	-3.6×10^{-6} ($\pm 3.7 \times 10^{-7}$) **10.2**	-3.0×10^{-6} ($\pm 3.2 \times 10^{-7}$) **10.5**	-4.0×10^{-6} ($\pm 2.8 \times 10^{-7}$) **7.0**
	Ethanol (1158)	-3.4×10^{-6} ($\pm 6.9 \times 10^{-7}$) **20.2**	-2.2×10^{-6} ($\pm 5.4 \times 10^{-7}$) **24.5**	-5.0×10^{-6} ($\pm 1.2 \times 10^{-6}$) **24.6**
	Octane (1316)	-6.2×10^{-6} ($\pm 1.5 \times 10^{-6}$) **23.6**	-5.0×10^{-6} ($\pm 9.6 \times 10^{-7}$) **19.1**	-5.8×10^{-6} ($\pm 2.0 \times 10^{-6}$) **34.3**

Notes: Three replicates were used to calculate the RSD for each pair (VOC and polymer-coated microcantilever), and only octane was used to assess intra-run repeatability. Water vapour did not react with PAA at this concentration therefore no signal was extracted.

concentrations, as shown between the polar mixture and non-polar mixture at 40%, in contrast to the mixtures at 20% and 30%.

Although we can predict a known interaction occurs such as electrostatic interactions based on VOC polarity (as described above), in reality there may be several additional interactions that take place with either a large or small impact on $\Delta f/f0$. One such impact is the viscosity of the polymer at room temperature, where morphological transition of the polymer layer from a 'glassy' state to a 'swollen' state may result in a changed damping effect on the micro-cantilever. Polymer chain length and ambient temperature may also be influencing factors on $\Delta f/f0$ signal. Additionally, experimental influences on $\Delta f/f0$ signal may arise from the amount of time required to adequately clean micro-cantilevers for subsequent runs, or from previous VOCs that remain on the micro-cantilevers where the size or effectiveness of the polymer surface has altered. It is possible that irreversible reactions occur between VOCs and cantilevers which may reduce the number of chemical binding sites.

Measurements of uncertainty for validated GC-MS analysis of pure standards vary from 2% to 19% for standard chemical VOCs trapped on sorbent material (Basanta *et al* 2012a, Mleth *et al* 2010, Mochalski *et al* 2014), with a general acceptance level for GC-MS metabolomic research of <30% (Dunn *et al* 2011). No such standard is available for micro-cantilever devices. It was therefore necessary to assess the reproducibility of measurements within and between runs, and between cantilevers. With regard to the reproducibility tests, although the sample size was small, results show that two different micro-cantilevers coated with the same polymer differ in $\Delta f/f0$ readings, which suggests polymer coating or micro-cantilever fabrication methods require further development to improve reproducibility. As the RSD values are high

for non-biological samples this can represent a high variation in ppmv terms. A calibration measurement may also be required prior to sample analysis.

Several strengths and limitations were identified throughout this work. Although not able to offer the same level of reproducibility and sample resolution as mass-spectrometry based instruments, the sensor system used in this study is compact, portable, a fraction of the cost of GC-MS analysers, and has a lower detection limit of 5 ppmv using acetone on PAA (sensitivity of 0.2 Hz ppm^{-1}). Although this detection limit was comparatively less than other studies and dependent on the gas delivery set up, it was achieved without pre-concentration, and further work would involve additional pre-concentration and reducing the synthesizer step size, where both would improve the sensitivity of detection. However, pre-concentration may reduce the potential real-time analysis capability of the sensor. The lack of selectivity may also impact the accuracy of acquired data. Future studies may use an enhanced gas delivery setup where VOCs are sampled in parallel or introduce water vapour (as breath is humid) when analysing VOCs to observe the effect of humidity on VOC differentiation. This can be achieved by using synthetic air instead of N_2 as CO2 can dissolve in humidity, which may cause reproducibility issues for sensor polymers. In addition, as breath gas is near 100% humidity, a water purging or heated permeable membrane may be required to avoid saturating the sensor polymers. To add to this, humidified air is less dense than dry air which can explain humidity measurement issues in addition to polymer absorption.

It is important to note that sensor chips can hold an array of polymer coated micro-cantilevers (from tens to hundreds), each with a chosen polymer coating to interact with a targeted set of VOCs, generating a detailed 'breathprint', and can theoretically be replaced by the operator with ease. Sensor chips can be tailored for different disease types or personalised

depending on patient characteristics. The advantage here is that a high volume of sensor chips ready for immediate use may be batch produced, keeping manufacturing costs low. In addition to increasing sample size, several variations and replicates of a polymer coating would increase statistical significance and fingerprinting analysis. Complex VOCs may then be used, where the aim may be to show differences between functional groups or molecular mass.

The sigmoid curve fitting model was used as this provided several features that could be interpreted. Further investigations may include evaluating curve features such as *AP* and *SP*, as these could be directly linked to interactions between VOCs and the polymer layer. Other curve features may be extracted such as a 'desorption point' where the $\Delta f/f0$ returns to baseline. An exponential curve model may be used instead, where the coefficients describe the observation. Regarding real-time measurements, a delayed exponential fit would be more appropriate. In its current state, the system allows for further research on the optimal readout and data processing, and novel polymer coatings for highly selective chemical interactions.

Conclusions

In this study we have developed a MEMS-based device to measure VOCs in a gas sample. We show that with three polymer coated micro-cantilevers, we were able to differentiate between individual VOCs and between polar and non-polar mixtures. Micro-cantilever-derived resonant frequency fluctuations correlated with ambient temperature changes. Further work is required to develop sensor micro-cantilever reproducibility and validate long term measurement reprodu-cibility. Overall, we have demonstrated that a low cost, stand-alone micro-cantilever sensor is capable of detecting VOCs, although further experiments are required to determine whether this device can be used for routine VOC sample analysis.

Acknowledgments

ORCID iDs

Waqar M Ahmed https://orcid.org/0000-0003-1490-6391
Royston Goodacre https://orcid.org/0000-0003-2230-645X
Stephen J Fowler https://orcid.org/0000-0002-4524-1663

References

Ahmed W M, Lawal O, Nijsen T M, Goodacre R and Fowler S J 2017 Exhaled volatile organic compounds of infection: a systematic review *ACS Infectious Dis.* **3** 695–710

Alvarez M and Lechuga L M 2010 Microcantilever-based platforms as biosensing tools *Analyst* **135** 827–36

Amann A, de Lacy Costello B, Miekisch W, Schubert J, Buszewski B, Pleil J, Ratcliffe N and Risby T 2014 The human volatilome: volatile organic compounds (VOCs) in exhaled breath, skin emanations, urine, feces and saliva *J. Breath Res.* **8** 034001

Basanta M, Ibrahim B, Dockry R, Douce D, Morris M, Singh D, Woodcock A and Fowler S J 2012a Exhaled volatile organic compounds for phenotyping chronic obstructive pulmonary disease: a cross-sectional study *Respir. Res.* **13** 1–9

Basanta M, Ibrahim B, Douce D, Morris M, Woodcock A and Fowler S J 2012b Methodology validation, intra-subject reproducibility and stability of exhaled volatile organic compounds *J. Breath Res.* **6** 1–9

Basanta M, Jarvis R M, Xu Y, Blackburn G, Tal-Singer R, Woodcock A, Singh D, Goodacre R, Paul Thomas C L and Fowler S J 2010 Non-invasive metabolomic analysis of breath using differential mobility spectrometry in patients with chronic obstructive pulmonary disease and healthy smokers *Analyst* **135** 315–20

Beale D, Jones O, Karpe A, Dayalan S, Oh D, Kouremenos K, Ahmed W and Palombo E 2016 A review of analytical techniques and their application in disease diagnosis in breathomics and salivaomics research *Int. J. Mol. Sci.* **18** 1–26

Beauchamp J D and Pleil J D 2013 Simply breath-taking? Developing a strategy for consistent breath sampling *J. Breath Res.* **7** 1–3

Bessonneau V, Mosqueron L, Berrubé A, Mukensturm G, Buffet-Bataillon S, Gangneux J P and Thomas O 2013 VOC Contamination in hospital, from stationary sampling of a large panel of compounds, in view of healthcare workers and patients exposure assessment *PLoS One* **8** e55535

Biagini D *et al* 2017 Determination of volatile organic compounds in exhaled breath of heart failure patients by needle trap micro-extraction coupled with gas chromatography-tandem mass spectrometry *J. Breath Res.* **11** 047110

Bos L D J, Sterk P J and Schultz M J 2013 Volatile metabolites of pathogens: a systematic review *PLoS Pathogens* **9** 1–8

Bos L D J, Weda H, Wang Y, Knobel H H, Nijsen T M E, Vink T J, Zwinderman A H, Sterk P J and Schultz M J 2014 Exhaled breath metabolomics as a noninvasive diagnostic tool for acute respiratory distress syndrome *Eur. Respir. J.* **44** 188–97

Bos L D, Sterk P J and Fowler S J 2016 Breathomics in the setting of asthma and chronic obstructive pulmonary disease *J. Allergy Clin. Immunol.* **138** 970–6

Chen H I and Chang K C 1991 Assessment of threshold and saturation pressure in the baroreflex function curve: a new mathematical analysis *Japan. J. Physiol.* **41** 861–77

de Lacy Costello B, Amann A, Al-Kateb H, Flynn C, Filipiak W, Khalid T, Osborne D and Ratcliffe N M 2014 A review of the volatiles from the healthy human body *J. Breath Res.* **8** 014001

de Vries R, Brinkman P, van der Schee M P, Fens N, Dijkers E, Bootsma S K, de Jongh F H C and Sterk P J 2015 Integration of electronic nose technology with spirometry: validation of a new approach for exhaled breath analysis *J. Breath Res.* **9** 1–10

Dekkers M, Nguyen M D, Steenwelle R, Te Riele P M, Blank D H A and Rijnders G 2009 Ferroelectric properties of epitaxial Pb(Zr, Ti)O$_3$ thin films on silicon by control of crystal orientation *Appl. Phys. Lett.* **95** 12902–2412

Dunn W B *et al* 2011 Procedures for large-scale metabolic profiling of serum and plasma using gas chromatography and liquid chromatography coupled to mass spectrometry *Nat. Protocols* **6** 1060–83

Fu J L and Ayazi F 2010 Dual-mode piezo-on-silicon resonant temperature and humidity sensor for portable air quality monitoring systems *Proc. IEEE Sens.* pp 2131–5

Ghimenti S *et al* 2013 Monitoring breath during oral glucose tolerance tests *J. Breath Res.* **7** 017115

Gromski P S, Correa E, Vaughan A A, Wedge D C, Turner M L and Goodacre R 2014 A comparison of different chemometrics

approaches for the robust classification of electronic nose data *Anal. Bioanal. Chem.* **406** 7581–90

Haick H and Cohen-kaminsky S 2015 Detecting lung infections in breathprints: empty promise or next generation diagnosis of infections *Eur. Respir. J.* **45** 21–4

Ibrahim B, Basanta M, Cadden P, Singh D, Douce D, Woodcock A and Fowler S J 2011 Non-invasive phenotyping using exhaled volatile organic compounds in asthma *Thorax* **66** 804–9

Konvalina G and Haick H 2014 Sensors for breath testing: from nanomaterials to comprehensive disease detection *Acc. Chem. Res.* **47** 66–76

Lange D, Hagleitner C, Hierlemann A, Brand O and Baltes H 2002 Cantilever arrays on a single chip: mass-sensitive detection of volatile organic compounds *Anal. Chem.* **74** 3084–95

Lourenço C and Turner C 2014 Breath analysis in disease diagnosis: methodological considerations and applications *Metabolites* **4** 465–98

Maute M, Raible S, Prins F E, Kern D P, Ulmer H, Weimar U and Gopel W 1999 Detection of volatile organic compounds VOCs with polymer-coated cantilevers *Sensors Actuators* B **58** 505–11

McDowall L M and Dampney R A 2006 Calculation of threshold and saturation points of sigmoidal baroreflex function curves *Am. J. Physiol. Heart Circ. Physiol.* **291** H2003–7

Miekisch W, Schubert J K and Noeldge-Schomburg G F E 2004 Diagnostic potential of breath analysis—focus on volatile organic compounds *Clin. Chim. Acta* **347** 25–39

Mleth M, Schubert J K, Gröger T, Sabei B, Kischkel S, Fuchs P, Hein D, Zimmermann R and Miekisch W 2010 Automated needle trap heart-cut GC/MS and needle trap comprehensive two-dimensional GC/TOF-MS for breath gas analysis in the clinical environment *Anal. Chem.* **82** 2541–51

Mochalski P, King J, Haas M, Unterkofler K, Amann A and Mayer G 2014 Blood and breath profiles of volatile organic compounds in patients with end-stage renal disease *BMC Nephrol.* **15** 1–14

Navazesh M 1993 Methods for collecting saliva *Ann. New York Acad. Sci.* **694** 72–7

Pettine J, Patrascu M, Karabacak D M, Vandecasteele M, Petrescu V, Brongersma S H, Crego-Calama M and Van Hoof C 2013 Volatile detection system using piezoelectric micromechanical resonators interfaced by an oscillator readout *Sensors Actuators* A **189** 496–503

Pettine J, Petrescu V, Karabacak D M, Vandecasteele M, Crego-Calama M and Van Hoof C 2012 Power-efficient oscillator-based readout circuit for multichannel resonant volatile sensors *IEEE Trans. Biomed. Circuits Syst.* **6** 542–51

Phillips M *et al* 2012 Point-of-care breath test for biomarkers of active pulmonary tuberculosis *Tuberculosis* **92** 314–20

Pleil J D, Stiegel M A and Risby T H 2013 Clinical breath analysis: discriminating between human endogenous compounds and exogenous (environmental) chemical confounders *J. Breath Res.* **7** 1–11

Rabis T, Sommerwerck U, Anhenn O, Darwiche K, Freitag L, Teschler H, Bödeker B, Maddula S and Baumbach J I 2011 Detection of infectious agents in the airways by ion mobility spectrometry of exhaled breath *Int. J. Ion Mobility Spectrom.* **14** 187–95

Rattray N J W, Hamrang Z, Trivedi D K, Goodacre R and Fowler S J 2014 Taking your breath away: metabolomics breathes life in to personalized medicine *Trends Biotechnol.* **32** 538–48

Smith D and Španel P 2005 Selected ion flow tube mass spectrometry (SIFT-MS) for on-line trace gas analysis *Mass Spectrom. Rev.* **24** 661–700

van Oort P M P *et al* 2017 BreathDx—molecular analysis of exhaled breath as a diagnostic test for ventilator–associated pneumonia: protocol for a European multicentre observational study *BMC Pulm. Med.* **17** 1–8

Waggoner P S and Craighead H G 2007 Micro- and nanomechanical sensors for environmental, chemical, and biological detection *Lab Chip* **7** 1238–55

White I R, Willis K A, Whyte C, Cordell R, Blake R S, Wardlaw A J, Rao S, Grigg J, Ellis A M and Monks P S 2013 Real-time multi-marker measurement of organic compounds in human breath: towards fingerprinting breath *J. Breath Res.* **7** 1–11

Wilson A 2015 Advances in electronic-nose technologies for the detection of volatile biomarker metabolites in the human breath *Metabolites* **5** 140–63

Wu C-H, Wang W-H, Hong C-C and Hwang K C 2016 A disposable breath sensing tube with on-tube single-nanowire sensor array for on-site detection of exhaled breath biomarkers *Lab Chip* **16** 4395–405

Xu P, Li X, Yu H, Liu M and Li J 2010 Self-assembly and sensing-group graft of pre-modified CNTs on resonant micro-cantilevers for specific detection of volatile organic compound vapors *J. Micromech. Microeng.* **20** 115003

Yoshikawa G, Lang H-P, Akiyama T, Aeschimann L, Staufer U, Vettiger P, Aono M, Sakurai T and Gerber C 2009 Sub-ppm detection of vapors using piezoresistive microcantilever array sensors *Nanotechnology* **20** 1–5